Effect of Horizontal Alternating Current Electric Field on the Stability of Natural Convection in a Dielectric Fluid Saturated Vertical Porous Layer

B. M. Shankar[1]
Department of Mathematics,
PES University,
Bangalore 560 085, India
e-mail: bmshankar@pes.edu

Jai Kumar
ISRO Satellite Centre,
Bangalore 560 017, India

I. S. Shivakumara
Department of Mathematics,
Bangalore University,
Bangalore 560 001, India

The stability of natural convection in a dielectric fluid-saturated vertical porous layer in the presence of a uniform horizontal AC electric field is investigated. The flow in the porous medium is governed by Brinkman–Wooding-extended-Darcy equation with fluid viscosity different from effective viscosity. The resulting generalized eigenvalue problem is solved numerically using the Chebyshev collocation method. The critical Grashof number G_c, the critical wave number a_c, and the critical wave speed c_c are computed for a wide range of Prandtl number Pr, Darcy number Da, the ratio of effective viscosity to the fluid viscosity Λ, and AC electric Rayleigh number R_{ea}. Interestingly, the value of Prandtl number at which the transition from stationary to traveling-wave mode takes place is found to be independent of R_{ea}. The interconnectedness of the Darcy number and the Prandtl number on the nature of modes of instability is clearly delineated and found that increasing in Da and R_{ea} is to destabilize the system. The ratio of viscosities Λ shows stabilizing effect on the system at the stationary mode, but to the contrary, it exhibits a dual behavior once the instability is via traveling-wave mode. Besides, the value of Pr at which transition occurs from stationary to traveling-wave mode instability increases with decreasing Λ. The behavior of secondary flows is discussed in detail for values of physical parameters at which transition from stationary to traveling-wave mode takes place.
[DOI: 10.1115/1.4029348]

Keywords: natural convection, heat transfer, porous layer, AC electric field, stability, Chebyshev collocation method

1 Introduction

In the recent past, several studies have addressed the stability of fluid flows in a fluid saturated porous medium. All these contributions, for instance, Makinde [1], Hill and Straughan [2], and Straughan and Harfash [3] are, however, limited to the case of a horizontal layer of porous medium. Nonetheless, the stability of natural convection in a vertical fluid saturated porous layer is important in analysis of natural convection flow arising from a heated impermeable surface, embedded in fluid saturated porous media, and has been used to model the heating of groundwater in an aquifer by a dike, which is idealized as a vertical impermeable surface. Besides, the study is of importance in many engineering and technological areas. These includes high performance insulation for building and cold storage, cooling of nuclear fuel in shipping flasks and water filled storage bays, insulation of high temperature gas cooled reactor vessels, burying of drums containing heat generating chemicals in the earth, regenerative heat exchangers containing porous materials, and so on. The instability of buoyancy opposed mixed convection in a vertical channel filled with a fluid-saturated porous medium is studied by Bera and Khalili [4].

Moreover, the influence of magnetic field or electric field becomes important as many fluid dynamical systems occurring in nature and engineering applications often involve electrically conducting fluids. In particular, the effects of magnetic field become dominant on convective instability when the fluid is either finitely or highly electrically conducting. Thermal convective instability in a horizontal electrically conducting fluid layer in the presence of a uniform vertical magnetic field has been studied in detail by Chandrasekhar [5]. Its counterpart in a porous medium has also been investigated in the past (Ref. [6] and references therein). The effect of temperature modulation on the onset of thermal convection in an electrically conducting fluid-saturated porous medium subjected to a vertical magnetic field is discussed by Bhadauria [7]. Bhatta et al. [8] studied steady magnetoconvection in a horizontal mushy layer, which is considered as a porous medium. To the contrary, if the fluid is dielectric then the electric forces play a major role rather than magnetic forces in driving the motion.

The effect of AC as well as DC electric fields on convective instability in a dielectric horizontal fluid layer has been studied extensively in the past [9–12]. In dielectric fluids, an applied temperature gradient produces nonuniformities in the dielectric constant. The variation in dielectric constant and the electric field intense the polarization force causing fluid motion. In this case, convection can occur in a dielectric fluid layer even if the temperature gradient is stabilizing (i.e., cooling from below and heating from above) and such an instability produced by an electric field is called electroconvection, which is analogous to Rayleigh–Bénard instability. In addition, if the applied temperature gradient is also destabilizing (that is, heating from below and cooling from above) then such an instability problem is called electrothermal convection.

The drying process in porous media is a rather complicated process and new techniques are on anvil to make the drying processes more efficient and one of the effective ways to improve the overall drying kinetics is to apply an electric field [13,14]. Besides, it is observed that imposing AC currents facilitate transport-related

[1]Corresponding author.

Contributed by the Heat Transfer Division of ASME for publication in the JOURNAL OF HEAT TRANSFER. Manuscript received June 21, 2014; final manuscript received December 4, 2014; published online January 7, 2015. Assoc. Editor: Zhixiong Guo.

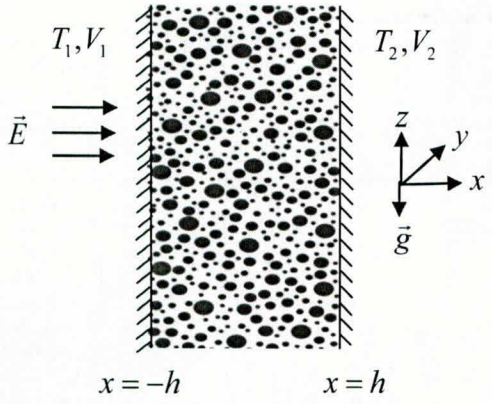

Fig. 1 Physical configuration

effects of two-phase flows, oil and water, in porous rocks [15]. It is thus imperative to study the stability of natural convection in a dielectric layer of porous medium in the presence of an electric field. The works which have been carried out in this direction are mainly concerned with buoyancy driven convection in a horizontal dielectric fluid saturated porous layer [15–17].

In this paper, the effect of a uniform AC electric field on the stability of natural convection in a vertical layer of dielectric fluid saturated sparsely packed porous medium is investigated because of its relevance and importance in many practical problems cited above. The resulting eigenvalue problem is solved numerically using Chebyshev collocation method and the results are presented graphically.

2 Mathematical Formulation

The physical configuration is as shown in Fig. 1. It consists of a Boussinesq dielectric fluid-saturated sparsely packed vertical layer of porous medium subject to a uniform AC electric field applied across the porous layer. A Cartesian coordinate system (x, y, z) is chosen with the origin at the middle of the vertical porous layer, where the x-axis is taken perpendicular to the plates and the z-axis is vertically upward, opposite in the direction of gravity. The plate at $x = -h$ is maintained at fixed temperature T_1 and fixed electric potential $V_1 (= 0)$, while the plate at $x = h$ is maintained at fixed temperature $T_2 (> T_1)$ and at an alternating (60 Hz) potential whose root-mean-square value is V_2. The equation of state is assumed to be linear

$$\rho(T) = \rho_0\{1 - \alpha(T - T_0)\} \tag{1}$$

where ρ_0 is the density at reference temperature $T = T_0$ (at the middle of the channel) and α is the thermal expansion coefficient. The dielectric constant is assumed to be linearly dependent on temperature

$$\varepsilon(T) = \varepsilon_0\{1 - \gamma(T - T_0)\} \tag{2}$$

where γ (>0) is the thermal expansion coefficient of dielectric constant and is assumed to be small. For example, for 10 cs silicone oil, $\gamma = 2.86 \times 10^{-3}$ K^{-1} and $\varepsilon = 2.6 \times 10^{-11}$ Fm^{-1}.

The dielectric fluid in the presence of electric field experiences a body force $\mathbf{f}_e$, which can be expressed as [18]

$$\mathbf{f}_e = \rho_e \mathbf{E} - \frac{1}{2}(\mathbf{E}\cdot\mathbf{E})\nabla\varepsilon + \frac{1}{2}\nabla\left(\rho\frac{\partial\varepsilon}{\partial\rho}\mathbf{E}\cdot\mathbf{E}\right) \tag{3}$$

Here, $\mathbf{E}$ is the root-mean-square value of the electric field, ρ_e is the free charge density, and ε is the dielectric constant. In Eq. (3), the Coulomb force term $\rho_e\mathbf{E}$ is neglected and only the dielectrophoretic force term $(\mathbf{E}\cdot\mathbf{E})\nabla\varepsilon/2$ is retained [10]. It is seen that the dielectrophoretic force term depends on $(\mathbf{E}\cdot\mathbf{E})$ rather than $\mathbf{E}$. We scale lengths with h, time with $\varphi_p h^2/\nu$, velocity with κ/h, temperature with βh, electric field with $\gamma\beta h E_0$, and pressure with $\rho_0\kappa\nu/h^2$ and arrive at the following nondimensional equations, respectively, for the conservation of mass, momentum, and energy [17,19]

$$\nabla\cdot\mathbf{q} = 0 \tag{4}$$

$$\frac{\partial\mathbf{q}}{\partial t} + \frac{1}{\mathrm{Pr}}(\mathbf{q}\cdot\nabla)\mathbf{q} = -\varphi_p^2\nabla P + G\,\mathrm{Pr}\,\theta\hat{k} - \frac{1}{\mathrm{Da}}\mathbf{q} + \Lambda\nabla^2\mathbf{q} - \frac{R_{\mathrm{ea}}}{2}(\mathbf{E}\cdot\mathbf{E})\nabla\varepsilon \tag{5}$$

$$M\,\mathrm{Pr}\frac{\partial\theta}{\partial t} + (\mathbf{q}\cdot\nabla)\theta = \nabla^2\theta \tag{6}$$

with

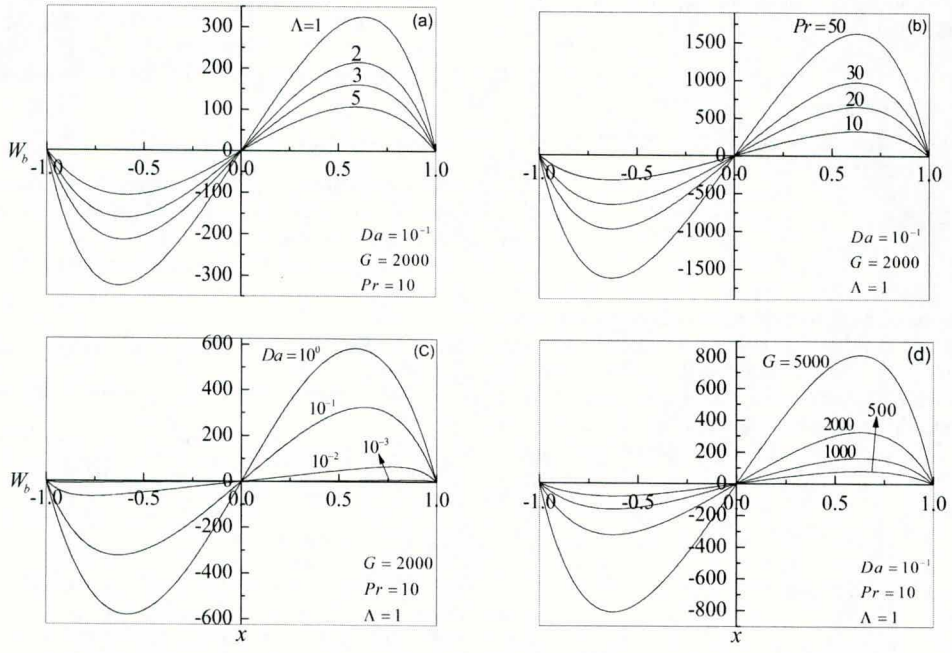

Fig. 2 Basic velocity profiles

Table 1 Order of base polynomial independency

	$\Lambda = 1, G = 1000, \mathrm{Pr} = 10, R_{ea} = 500,$ $a = 1.3, \mathrm{Da} = 10^0$		$\Lambda = 1, G = 5000, \mathrm{Pr} = 5, R_{ea} = 500,$ $a = 1.0, \mathrm{Da} = 10^{-1}$	
N	c_r	c_i	c_r	c_i
1	−1.06347688	18.55040886	−1.63863768	−50.04448946
5	−0.34802857	23.65207688	−0.65803884	−19.84774664
10	−0.23948191	25.00002772	−2.51750973	−0.00003551
15	−1.11422137	26.74831987	−2.38597731	−0.00014765
20	−1.11470659	26.74380337	−1.62687643	−0.00011241
25	−1.11471709	26.74385713	−1.62682867	−0.00014189
30	−1.11471985	26.74385061	−1.62682941	−0.00013953
35	−1.11471985	26.74385059	−1.62682943	−0.00013964
40	−1.11471986	26.74385059	−1.62682944	−0.00013964
50	−1.11471986	26.74385058	−1.62682944	−0.00013964
60	−1.11471986	26.74385059	−1.62682944	−0.00013963
70	−1.11471986	26.74385059	−1.62682944	−0.00013964
80	−1.11471986	26.74385059	−1.62682944	−0.00013964

$$\nabla \times \mathbf{E} = 0 \text{ or } \mathbf{E} = -\nabla V, \nabla \cdot (\varepsilon \mathbf{E}) = 0 \tag{7}$$

Here, $\mathbf{q} = (u, v, w)$ is the velocity vector, P is the modified pressure, $\theta (= T - T_0)$ is the temperature, V is the electric potential, R_{ea} is the AC electric Rayleigh number, Pr is the Prandtl number, G is the Grashof number, Λ is the ratio of effective viscosity to the fluid viscosity, Da is the Darcy number, M is a nondimensional group, and φ_p is the porosity of the porous medium.

3 Basic State

The basic state solution is found to be

$$\begin{aligned} W_b &= \frac{G\,\mathrm{Pr}\,\mathrm{Da}}{2}\left[x - \mathrm{cosech}\left(1/\sqrt{Da\Lambda}\right)\sinh\left(x/\sqrt{Da\Lambda}\right)\right], \\ \theta_b &= \frac{x}{2}, \quad \varepsilon_b = 1 - \frac{\Gamma x}{2}, \quad \mathbf{E}_b = \frac{1}{\Gamma}\left[\frac{1}{1 - \Gamma x/2}\right]\hat{i}, \\ V_b &= \frac{2}{\Gamma^2}\log\left(\frac{1 - \Gamma x/2}{1 + \Gamma/2}\right), \quad (\Gamma = \gamma\beta h) \end{aligned} \tag{8}$$

The pressure is of no consequence as we are eliminating the same. It should be noted that in the initial steady state the electric field does not affect the flow field.

4 Linear Stability Analysis

To study the stability of the basic state, we superimpose an infinitesimal disturbance on the base flow in the form

$$\begin{aligned} &\mathbf{q} = \mathbf{q}_b + \mathbf{q}', \quad P = P_b + P', \quad V = V_b + V', \\ &\theta = \theta_b + \theta', \quad \varepsilon = \varepsilon_b + \varepsilon' \end{aligned} \tag{9}$$

Equation (9) is substituted back in to Eqs. (4)–(7) and usual steps of linear stability theory is followed [19]. Since Squire's theorem is valid, we consider only two-dimensional flows, and hence, a stream function $\psi(x, z, t)$ is introduced through $u = \partial\psi/\partial z$ and $w = -\partial\psi/\partial x$. Then, the normal mode analysis procedure is applied in the form $\{\psi, \theta, V\} = \{\Psi, \Theta, \Phi\}(x)e^{ia(z-ct)}$, where $c = c_r + ic_i$ and a is the wave number, to arrive at the following stability equations:

$$\begin{aligned} &\left(\frac{W_b}{\mathrm{Pr}} - c\right)(D^2 - a^2)\Psi - \frac{1}{\mathrm{Pr}}D^2 W_B \Psi + \frac{R_{ea}}{2}(D\Phi + \Theta) \\ &\quad = \frac{1}{ia}\left[\Lambda(D^2 - a^2)^2\Psi - \frac{1}{\mathrm{Da}}(D^2 - a^2)\Psi - G\,\mathrm{Pr}\,D\Theta\right] \end{aligned} \tag{10}$$

$$\left(\frac{W_b}{\mathrm{Pr}} - Mc\right)\Theta + \frac{1}{2\,\mathrm{Pr}}\Psi = \frac{1}{ia\,\mathrm{Pr}}(D^2 - a^2)\Theta \tag{11}$$

$$D\Theta + (D^2 - a^2)\Phi = 0 \tag{12}$$

Equations (10)–(12) are to be solved subject to appropriate boundary conditions. It is considered that on the rigid and isothermal vertical plates the tangential electric field vanishes. Thus the associated boundary conditions are

$$\Psi = D\Psi = \Theta = \Phi = 0 \text{ at } x = \pm 1 \tag{13}$$

Equations (10)–(12) together with the boundary conditions (13) constitute an eigenvalue problem which has to be solved numerically. The resulting eigenvalue problem is solved using the Chebyshev collocation method. The numerical results reported are based on the leading eigenvalue of the said system. By this, we mean that when one employs the time representation in ψ, θ, and V of form e^{-iact} with $c = c_r + ic_i$ then this results in ψ, θ, and V having terms of form $e^{-iac_r t} \cdot e^{ac_i t}$. The eigenvalues are found such that the largest value of c_i is $c_i = 0$ and then the result is minimized over the wave number a. The resulting G value is then the critical Grashof number with corresponding wave number. The value $c_i = 0$ is chosen because this is the threshold at which the solution becomes unstable according to linearized theory. For, if $c_i > 0$ then ψ, θ, and V grow rapidly like $e^{ac_i t}$ and the solution is unstable.

5 Results and Discussion

A numerical study has been carried to analyze the effect of uniform horizontal AC electric field on the stability of natural convection in a dielectric fluid saturated vertical porous layer whose walls are maintained at constant but different temperatures. The Brinkman–Wooding-extended Darcy model is adopted to describe

Table 2 Variation of G_c, a_c, and c_c as a function of Pr for $R_{ea} = 0 = 1/\mathrm{Da}$, $M = 1$

Pr	G_c	a_c	c_c
1.0	992.52946472	1.404	0
5.0	982.99195862	1.384	0
10.0	983.55348200	1.383	0
12.6	984.09135449	1.383	0
12.7	984.09135447	1.383	0
12.8	831.82237442	0.400	±24.83007796
13.0	769.99223337	0.420	±23.04185671
15.0	487.16752634	0.608	±14.72510713
20.0	301.71983348	0.820	±9.29210134

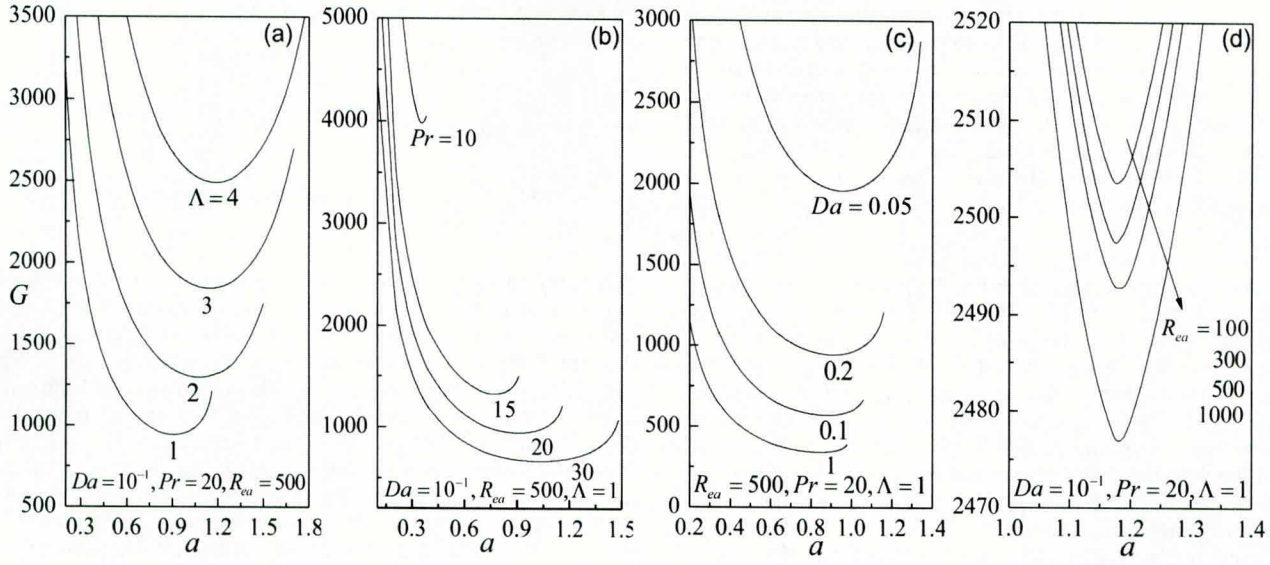

Fig. 3 Neutral stability curves

the flow in a porous medium. The solution obtained for the basic flow reveals that R_{ea} has no influence on the basic flow but the other parameters Λ, Pr, Da, and G alters the same significantly. Figures 2(*a*)–2(*d*), respectively, show the influence of Λ, Pr, Da, and G on the basic velocity W_b. These figures indicate that decrease in the value of Pr, Da, and G (Figs. 2(*b*)–2(*d*)) is to suppress the fluid flow but a similar trend is noticed with increasing Λ (Fig. 2(*a*)). These figures indicate that the velocity profiles are antisymmetric about the vertical line at $x = 0$. However, they are not precisely centrosymmetric about $x = \pm 1/2$. Further inspection of the figures reveals that increase in Pr, Da, and G while decrease in Λ lead to the formation of thin boundary layers near the two vertical walls.

To know the accuracy of the numerical method employed, the number of terms in the collocation method was increased. It is observed that the results remain consistent with an improved accuracy for all the parametric values considered by taking 61 terms in the Chebyshev collocation method (Table 1). In order to validate our numerical results, test computations were performed considering 61 terms under the limiting case of $R_{ea} = 0 = 1/\mathrm{Da}$ for different values of Pr and for $M = 1$. The critical Grashof number G_c, the critical wave number a_c, and the critical wave speed c_c computed numerically are tabulated in Table 2. From the table, it is observed that the transition from stationary to traveling-wave mode occurs when the Prandtl number Pr exceeds the value 12.7 which is in agreement with the well established results in Refs. [19–21].

Figures 3(*a*)–3(*d*) demonstrate the neutral curves on the (G, a)-plane for various values of Λ, Pr, Da, and R_{ea}, respectively. In the calculation, the value of M is fixed at 1. In these figures, the portion below each neutral stability curve corresponds to stable region and the region above corresponds to instability. It is seen that the neutral stability curves exhibit single but different minimum with respect to the wave number for various values of Λ, Pr, Da, and R_{ea}. From Fig. 3(*a*), it is observed that the effect of increasing Λ is to increase the region of stability, while an opposite trend is noticed with increasing Pr (Fig. 3(*b*)). Figure 3(*c*) exhibits that increasing Da is to decrease the region of stability and a similar effect could be seen with increasing R_{ea} and the same is evident from Fig. 3(*d*).

The critical stability parameters G_c, c_c, and a_c are computed for different values of physical parameters to know their impact on the stability characteristics of the system. Figure 4(*a*) shows the variation of G_c with Pr for different values of Da when $\Lambda = 1$ and $R_{ea} = 500$. It is important to note that the mode of instability changes with increasing Pr. There is a general reduction in the origin of the curves as the reference Da value increases. For

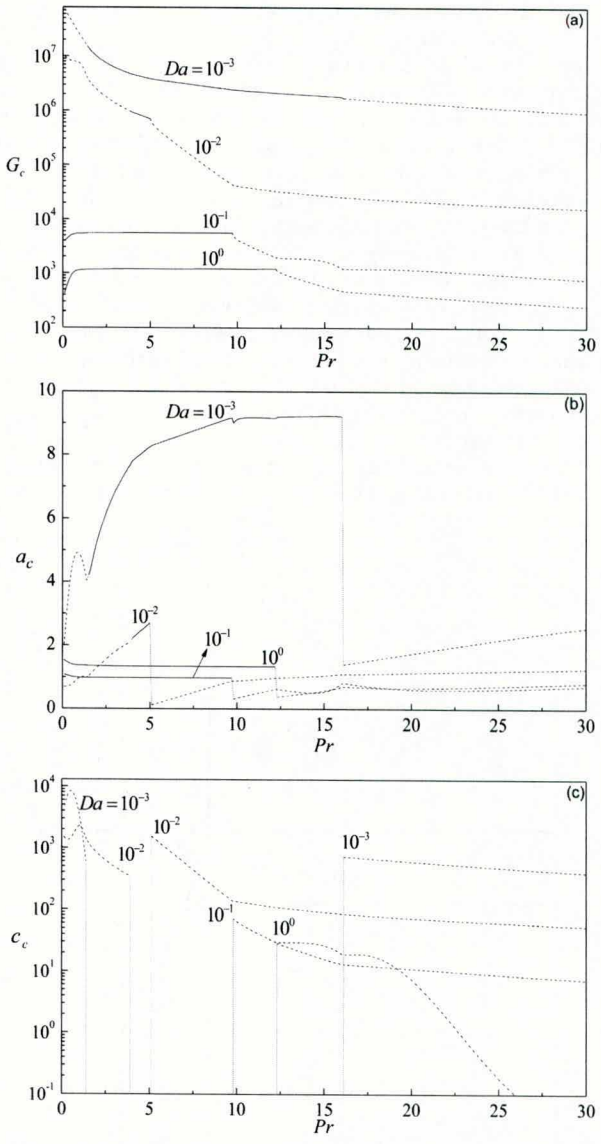

Fig. 4 Variation of (*a*) G_c, (*b*) a_c, and (*c*) c_c with Pr for a fixed value of R_{ea} (=500), Λ(=1) and for various values of Da. (——) Stationary modes, (·····) traveling-wave modes.

$Da = 10^{-3}$, there is a sheer drop in the curve and as the curve progresses there is a reduction in its slope. The same can be seen for $Da = 10^{-2}$, except for the initial drop to be steeper when compared to the previous curve. Further, it is seen that the instability is via traveling-wave mode for low values of Pr when $Da = 10^{-3}$ and switches over to stationary up to $Pr = 16$. With further increase in Pr, the instability transits back to the traveling-wave mode. Similar pattern (traveling-wave to stationary and again to traveling-wave mode) is observed for $Da = 10^{-2}$. Interestingly, the flow is predominantly traveling-wave mode, while it is stationary for a very short interval at low Pr values. As Da approaches larger multiples of 10 (i.e., $Da = 10^{-1}$ and 10^{0}), there is perceptible difference in the behavior of the curves. For both the values of Da, the curves are fairly constant and the instability switches over from stationary to traveling-wave mode at some threshold value of Pr. Such a weak influence of Pr on G_c at stationary mode is another indication that buoyancy forces are the dominant source of instability. But they experience a drop in G_c with increasing Pr. In other words, the Prandtl number shows no significant effect if the disturbances are stationary, while its effect is significant if the disturbances are via traveling-wave modes. From Fig. 4(*a*), it is also noticed that decrease in the value of Da is to increase the value of G_c and thus it has a stabilizing effect on the system. This may be attributed to the fact that decreasing Da amounts to decrease in the permeability of the porous medium, which in turn retards the fluid flow.

Figure 4(*b*) illustrates the variation of a_c as a function of Pr for different values of Da when $\Lambda = 1$ and $R_{ea} = 500$. These graphs show irregular behavior for different reference Da values. With $Da = 10^{-3}$, there is a sharp rise in the graph, for lower values of Pr. As Pr approaches the value 16, a vertical drop followed by a gradual rise in the curve is observed. For values of Pr lesser than 10 and at $Da = 10^{-2}$, the curve rises and falls in a triangular fashion and increases gradually to almost a horizontal curve thereafter. Curves for $Da = 10^{-1}$ and 10^{0} show similar behavior. The curves are of constant a_c values in the stationary mode, and after undergoing a mild drop, continue to move as horizontal curves. Corresponding c_c summarized in Fig. 4(*c*), indeed confirm the above observed behavior more evidently. The vertical lines represent the discontinuous changes in c_c due to the transition from stationary to traveling-wave mode.

Furthermore, streamlines and isotherms at the critical state for both stationary and traveling-wave modes are analyzed. The stream lines and isotherms are drawn, respectively from the following expressions:

$$\Psi = \sum_{j=0}^{N} \left(\mathrm{Re}(\Psi_j)\cos az - \mathrm{Im}(\Psi_j)\sin az\right)\xi_j(x),$$
$$\Theta = \sum_{j=0}^{N} \left(\mathrm{Re}(\Theta_j)\cos az - \mathrm{Im}(\Theta_j)\sin az\right)\xi_j(x) \tag{14}$$

where Ψ_j's and Θ_j's are the eigenvectors and $\xi_j(x)$ is a Chebyshev polynomial of order j. In all contour plots, dashed lines denote negative values whereas solid lines stand for positive values. Figures 5 and 6 show the results for different values of Pr when $\Lambda = 1$, $R_{ea} = 500$, and $Da = 10^{-1}$. The streamlines and isotherms are shown in Figs. 5(*a*)–5(*d*) and 6(*a*)–6(*d*), respectively, for $Pr = 3.8$, 4.0, 4.9, and 5.1. The pattern appears to be stationary bicellular convection in streamlines, whereas in isotherms similar to bicellular oblate triangles are observed. It is also observed that the magnitude of secondary flow is very weak. Nonetheless, it is seen that the flow strength suddenly changes only qualitatively but not quantitatively in both streamlines and isotherms once the value of Pr increases from 9.6 (Figs. 5(*e*) and 6(*e*)) to 9.8 (Figs. 5(*f*) and 6(*f*)). Also, there is a sudden increase in wavelength and this confirms that transition mode occurs at that point.

Figures 7(*a*)–7(*f*) exhibit the evolution of streamline patterns for various values of Pr when $\Lambda = 1$, $R_{ea} = 500$, and $Da = 10^{-2}$. For $Pr = 3.8$, the streamlines are concentrated at the geometrical center of the fluid cross section and mild ripples are observed toward the left (Fig. 7(*a*)). The streamlines shown in Fig. 7(*b*) for $Pr = 4.0$, the value at which transition from traveling-wave to stationary mode takes place, are more or less mirror image of streamlines presented in Fig. 7(*a*) for $Pr = 2$ but the strength of the secondary flow is found to increase marginally. The streamlines shown in Fig. 7(*c*) for an increased value of $Pr = 4.9$ reveals that the undulations observed in Figs. 7(*a*) and 7(*b*) seem distributed on either sides of the origin. The flow pattern and flow strength changes qualitatively as well as quantitatively as the instability changes from stationary to traveling-wave mode with further increase in the value of Pr. In other words, the instability switches over from stationary to traveling-wave mode once the value of Pr exceeds the value 5.0. When $Pr = 5.1$, it is observed that the convective motion is constructed by two parts, one is the vigorous cell in the right half of

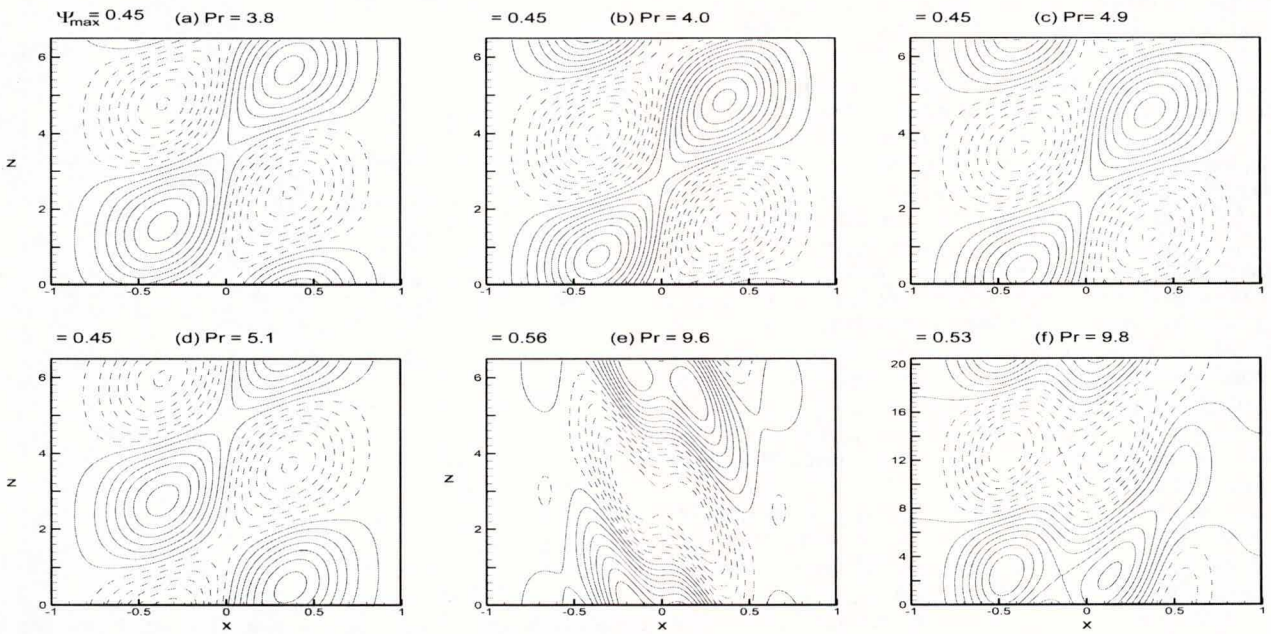

Fig. 5 The disturbance streamlines for different values of Pr when $\Lambda = 1$, $R_{ea} = 500$, and $Da = 10^{-1}$

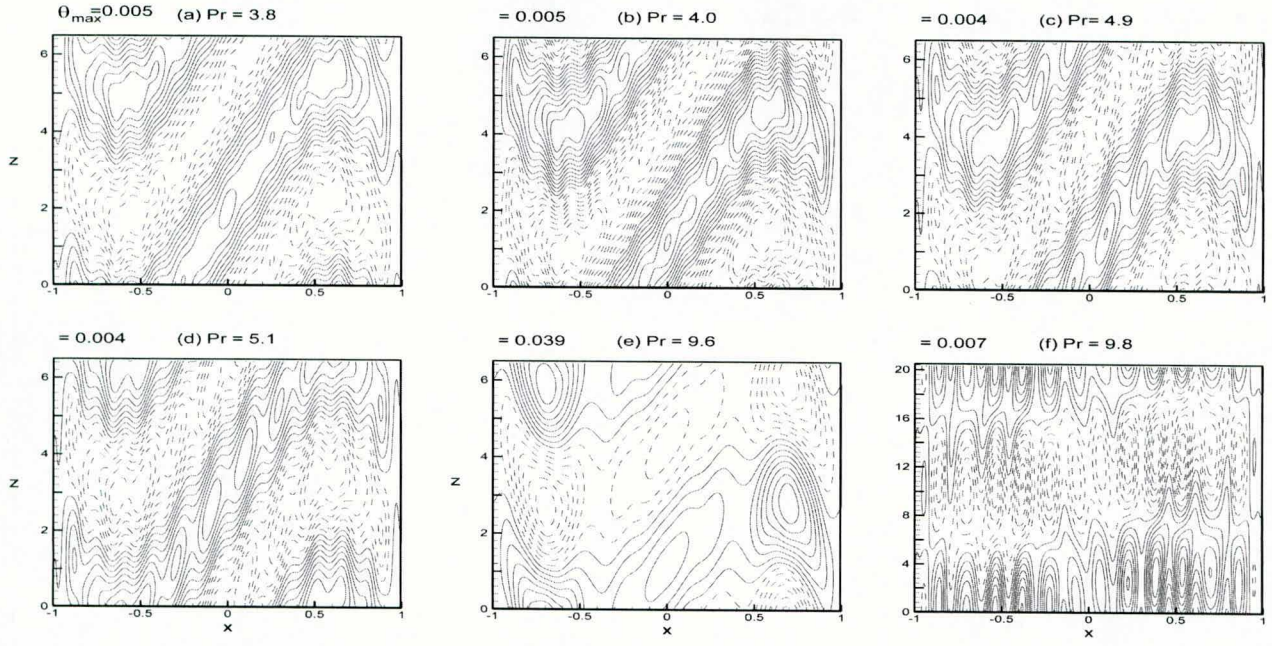

Fig. 6 The disturbance isotherms for different values of Pr when $\Lambda = 1$, $R_{ea} = 500$, and $Da = 10^{-1}$

the porous layer adjacent to the right surface, the other is the weak circulation which is exterior to the vigorous convection cell. This is evident from Fig. 7(*d*). It is further seen that the actual wavelengths are substantially larger in streamlines and at this stage Ψ_{max} increases from 0.41 to 0.69. Further increase in Pr is to decrease the wavelength and increase in flow strength (Figs. 7(*e*) and 7(*f*)).

Figures 8(*a*) and 8(*b*) illustrate the variation of G_c and a_c as a function of Pr for different values of R_{ea} when $\Lambda = 1$ and $Da = 10^{-1}$. Figure 8(*a*) reveals that the magnitude of the basis of the curve and the peaks increase as R_{ea} increases at lower values of $Pr(< 1)$. Further increase in Pr, the peak disappears and the curves for all values of R_{ea} come together up to $Pr = 9.7$. Thereafter, there is a vertical followed by a parabolic drop in the G_c value for all the values of R_{ea}. In other words, Pr shows no significant effect if the disturbances are stationary. This may be due to the fact that the energy for stationary instability at low to moderate Pr is derived mainly from the base flow velocity field through the action of disturbance Reynolds stresses at the midplane between the upward and the downward flowing convective streams. Whereas the effect of Pr becomes significant if the disturbances are traveling-wave mode. Although the effect of increasing R_{ea} is to instill instability on the system but its influence is found to be not so significant. That is, higher the electric field strength the less stable the system due to an increase in the destabilizing electrostatic energy to the system. Figure 8(*b*) demonstrates that the origin of the curve is lower for lower values of R_{ea} and increases with the latter for $Pr < 1$. Further, the curves of different Pr and R_{ea} coalesce until $Pr = 9.7$ and then there is a sudden massive drop in its value and it then increases almost logarithmically. This indicates two different physical mechanisms of instability. As Pr increases, there is a tendency for more of the disturbance energy to originate from the potential energy associated with the buoyancy effect than as transfer from the kinetic energy of the base flow by the action of Reynolds stresses.

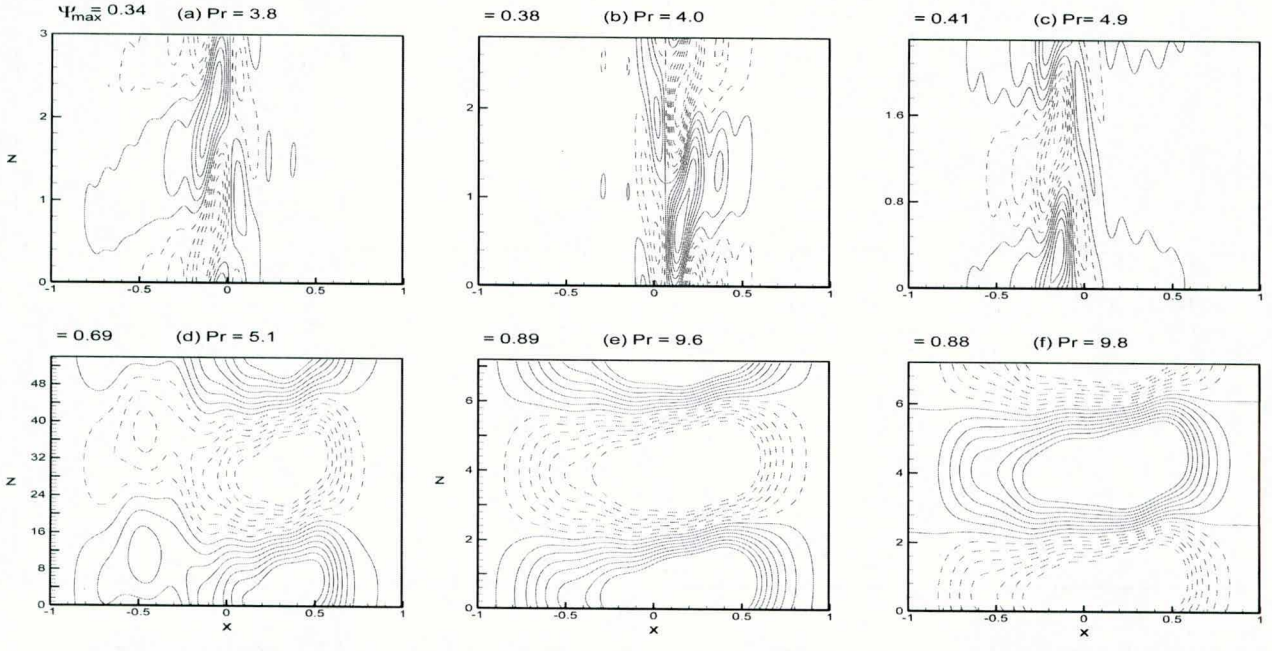

Fig. 7 The disturbance streamlines for different values of Pr when $\Lambda = 1$, $R_{ea} = 500$, and $Da = 10^{-2}$

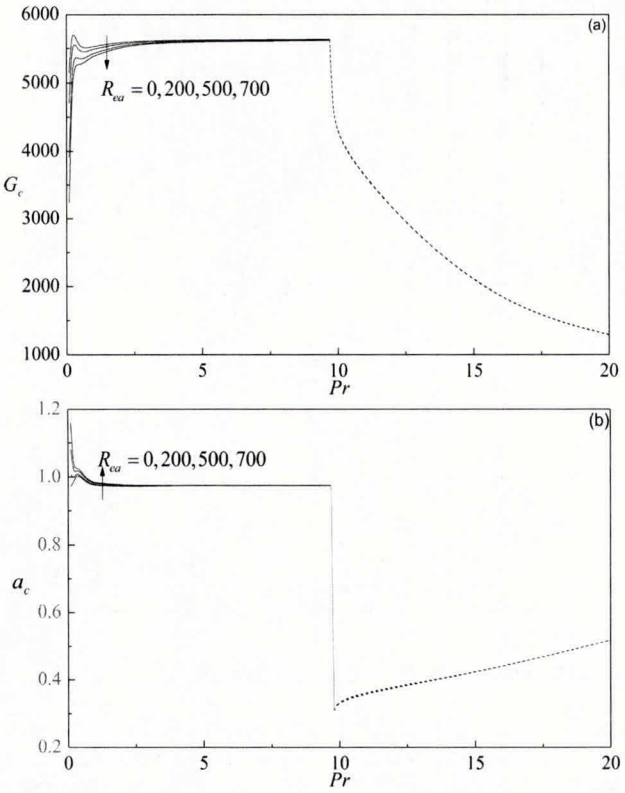

Fig. 8 Variation of (*a*) G_c and (*b*) a_c with Pr for a fixed value of Da($=10^{-1}$), $\Lambda(=1)$ and for various values of R_{ea}. (——) Stationary modes and (·····) traveling-wave modes.

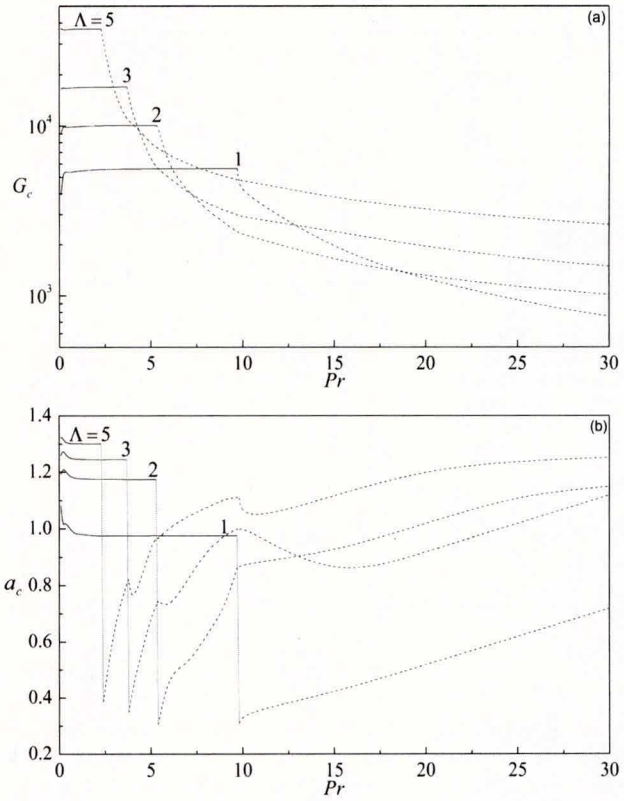

Fig. 10 Variation of (*a*) G_c and (*b*) a_c with Pr for a fixed value of R_{ea}(=500), Da($=10^{-1}$) and for various values of Λ. (——) Stationary modes and (·····) traveling-wave modes.

To know the influence of Pr and R_{ea} on the disturbance flow and temperature, the corresponding streamlines and isotherms at the critical state for both stationary and traveling-wave modes are displayed in Fig. 9 for different values of Pr when $\Lambda = 1$, $R_{ea} = 200$, and Da $= 10^{-1}$. For Pr $= 5$ and 9.6, the flow pattern appears to be stationary bicellular in both streamlines and isotherms as shown in Figs. 9(*a*), 9(*b*) and 9(*e*), 9(*f*), respectively. An abrupt change could be seen in stability profile as the instability mode changes from stationary to traveling-wave mode. Here, the flow pattern changes qualitatively but not quantitatively as the mode changes from stationary to traveling-wave mode. In other words, the instability switches over from stationary to traveling-wave mode once the value of Pr exceeds 9.6. When Pr $= 9.8$, convective cells transform into unicellular from bicellular in streamlines (Fig. 9(*c*)). In

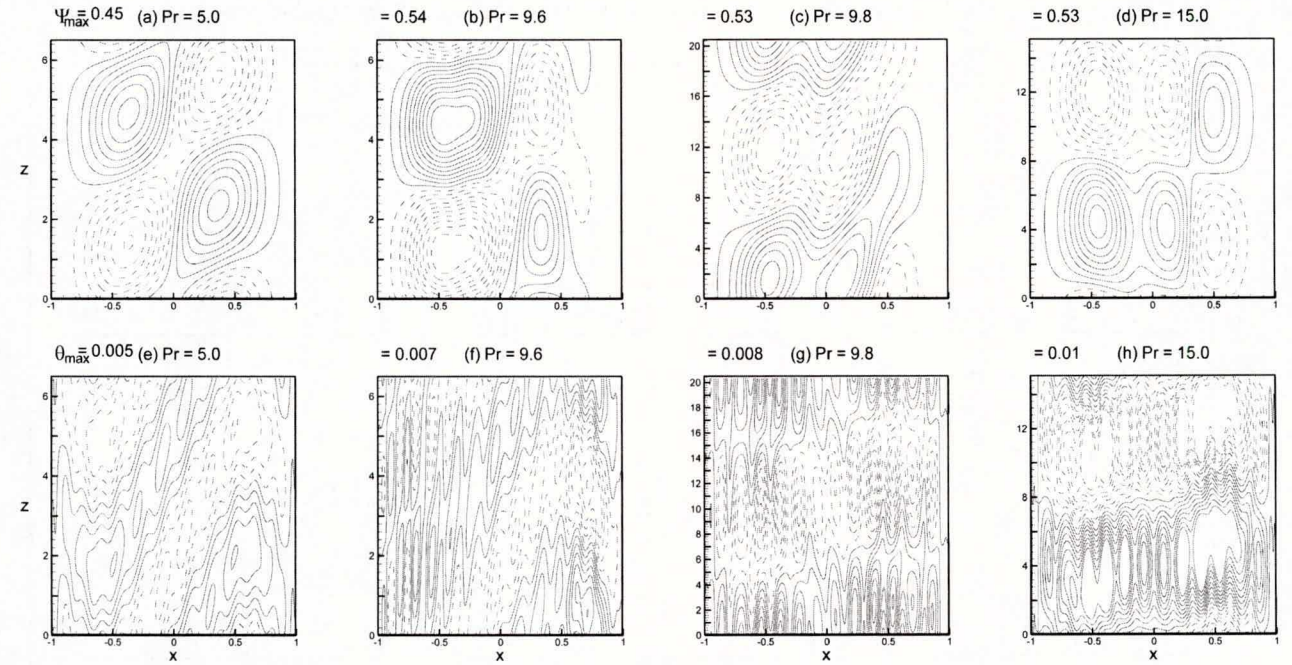

Fig. 9 The disturbance streamlines (*a*)–(*d*) and isotherms (*e*)–(*h*) for different values of Pr when $\Lambda = 1$, Da $= 10^{-1}$, and $R_{ea} = 200$

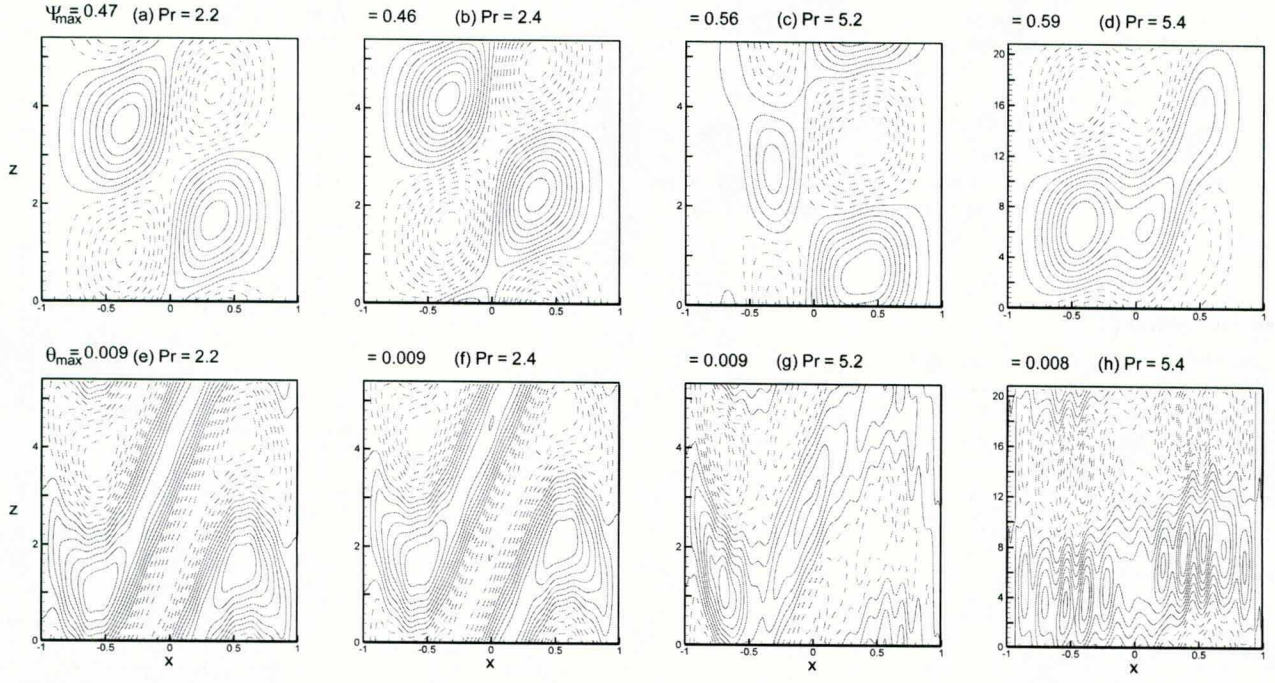

Fig. 11 The disturbance streamlines (*a*)–(*d*) and isotherms (*e*)–(*h*) for different values of Pr when $\Lambda = 2$, $\mathrm{Da} = 10^{-1}$, $R_{ea} = 500$

isotherms, a flurry of activity is noticed as observed in Fig. 9(*g*). Cells of various patterns and shapes are seen throughout the spread of the porous layer. Similar behavior is observed in both streamlines and isotherms when $\mathrm{Pr} = 15$ (Figs. 9(*d*) and 9(*h*)). It is also observed that the change in streamline and isotherm patterns remains unaltered with increasing values of R_{ea}.

The porous materials used in many technological applications of practical importance possess high permeability values. For example, permeabilities of compressed foams as high as 8×10^{-6} m^2 and for a 1 mm thick foam layer the equivalent Darcy number is equal to 8 (see Ref. [22] and references therein). Moreover, for such a high porosity porous medium, Givler and Altobelli [23] determined experimentally that $\mu_e = 7.5^{+3.4}_{-2.4}\mu$, where μ_e is the effective viscosity or the Brinkman viscosity and μ is the fluid viscosity. Therefore, the ratio of these two viscosities is considered to be different from unity in analyzing the problem. The variation of G_c, a_c, and c_c with Pr is shown in Fig. 10 for different values of Λ when $R_{ea} = 500$ and $\mathrm{Da} = 10^{-1}$. Depending on the value of Λ, there exists a threshold value of Pr at which the instability switches over from stationary to traveling-wave mode (Fig. 10(*a*)). Moreover, the threshold value of Pr increases noticeably with decreasing Λ. In the stationary mode, decreasing Λ will lead to the decrease in G_c and thus it has a destabilizing effect on the system. This is because, increasing Λ amounts to increase in the viscous effect, which in turn retards the fluid flow. However, Λ shows a dual behavior on G_c if the instability is via traveling-wave mode. It is also seen from the figure that the dependence of G_c upon Pr is very weak in the case of stationary mode, while G_c at traveling-wave mode is a strongly decreasing function of Pr. The vertical lines represent discontinuous changes in a_c due to the transition from stationary to traveling-wave mode (Fig. 10(*b*)). It is evident from the figure that the dependence of a_c at stationary mode upon Pr is weak, whereas a_c at traveling-wave mode depends strongly upon Pr. It is also seen from Fig. 10(*b*) that as Λ decreases a_c decreases at stationary mode, whereas it exhibits a twin behavior at traveling-wave mode.

The streamlines and isotherms are displayed for representative values of physical parameters considered in Fig. 10. Figures 11(*a*)–11(*d*) and 11(*e*)–11(*h*) exhibit streamlines and isotherms before and after the transition mode as a function of Pr for $\Lambda = 2$, $\mathrm{Da} = 10^{-1}$, and $R_{ea} = 500$. For $\mathrm{Pr} = 2.2$, 2.4, and 5.2, the flow pattern appears to be as stationary and bicellular. Further, the streamlines move closer and appear to be parallel at the center of the vertical porous layer (Figs. 11(*a*)–11(*c*)). The corresponding isotherms are shown in Figs. 11(*e*)–11(*g*). It can be seen that bicellular oblate triangle cells occupy the whole thickness of vertical porous layer. The instability switches over from stationary to traveling-wave mode once the value of Pr exceeds the value 5.2. When $\mathrm{Pr} = 5.4$, convective cells transform into unicellular from bicellular in streamlines (Fig. 11(*d*)) whereas in isotherms, it appears as though the cells move out in a ripple like manner from the center of the fluid cross section (Fig. 11(*h*)). It is further seen that the actual wavelengths are substantially larger in both streamlines and isotherms. Interestingly, change in Ψ_{max} and θ_{max} is marginal at this stage. Same observations are noticed with increase in Λ at the critical state.

6 Conclusions

The following conclusions can be drawn from the foregoing study:

(i) Although the basic flow is independent of R_{ea}, it is significantly influenced by Λ, Pr, Da, and G.

(ii) The decrease in the value of Da is to reinforce stability on the system. A definite single threshold value of Pr exists denoting transition from stationary to traveling-wave mode for $\mathrm{Da} = 10^0$ and 10^{-1} and this threshold value increases as Da decreases. Nonetheless, for $\mathrm{Da} = 10^{-2}$ and 10^{-3}, there is an abrupt change in the flow pattern exists with increasing Pr (i.e., instability switches over from traveling-wave to stationary mode and again it transits back to traveling-wave mode). In other words, there is a range of Pr in which the instability is via stationary mode and this range of Pr increases with the decrease in the value of Da.

(iii) The ratio of viscosities Λ shows stabilizing effect on the system at the stationary mode. To the contrary, it exhibits a dual behavior if the instability is via traveling-wave mode. Moreover, the value of Pr at which transition occurs from stationary to traveling-wave mode increases as the value of Λ decreases.

(iv) Increase in the AC electric Rayleigh number R_{ea} is to destabilize the flow due to increasing destabilizing electrostatic energy but its effect is found to be not so significant. The

value of Pr at which transition from stationary to traveling-wave instability occurs and the critical wave number remain invariant for all values of AC electric Rayleigh number.

(v) The magnitudes of secondary flows (streamlines and isotherms) confirm the behavior of stability curves observed before and after the change of mode of instability. For the range of parametric values considered, convective cells are found to appear in unicellular, bicellular as well as multicellular in nature.

Acknowledgment

One of the authors B.M.S is indebted to Professor N. Rudraiah for his advice and encouragement during the course of this study. This work constitutes part of a Ph.D. thesis submitted to the Department of Mathematics in the Bangalore University, Bangalore. The authors wish to thank the reviewers for their constructive comments, which helped in improving the paper considerably.

Nomenclature

a = vertical wave number
c = wave speed
c_r = phase velocity
c_i = growth rate
D = differential operator
$\mathrm{Da} = K\varphi_p^2/h^2$ = Darcy number
$\mathbf{E}$ = root-mean-square value of the electric field
E_0 = root-mean-square value of the electric field at $x = 0$
$\mathbf{f}_e$ = force of electrical origin
$\mathbf{g}$ = acceleration due to gravity
$G = \alpha g \varphi_p^2 \beta h^4/\nu^2$ = Grashof number
h = thickness of the dielectric porous layer
$\hat{k}$ = unit vector in z-direction
K = permeability of the porous medium
P = modified pressure
$\mathrm{Pr} = \nu/\kappa$ = Prandtl number
$\mathbf{q} = (u, v, w)$ = velocity vector
$R_{\mathrm{ea}} = \gamma^2 \varphi_p^2 \varepsilon_0 E_0^2 \beta^2 h^4/\mu\kappa$ = AC electric Rayleigh number
t = time
T_1 = temperature of the left boundary
T_2 = temperature of the right boundary
V = root-mean-square value of the electric potential
V_1 = electric potential of the left boundary
V_2 = electric potential of the right boundary
W_b = basic velocity
(x, y, z) = Cartesian co-ordinates

Greek Symbols

α = volumetric thermal expansion coefficient
β = temperature gradient
γ = thermal expansion coefficient of dielectric constant
ε = dielectric constant
ε_0 = reference dielectric constant at T_0
θ = temperature
Θ = amplitude of perturbed temperature
κ = thermal diffusivity
$\Lambda = \varphi_p^2 \mu_e/\mu$ = ratio of effective viscosity to the fluid viscosity
μ = fluid viscosity
μ_e = effective viscosity
$\nu = \mu/\rho_0$ = kinematic viscosity
ρ = fluid density
ρ_e = free charge density
ρ_0 = reference density at T_0
σ = electrical conductivity of the fluid
$\mathbf{\Phi}$ = amplitude of perturbed electric potential
φ_p = porosity of the porous medium
χ = ratio of heat capacities
ψ = stream function
Ψ = amplitude of vertical component of perturbed velocity

References

[1] Makinde, O. D., 2009, "On the Chebyshev Collocation Spectral Approach to Stability of Fluid Flow in a Porous Medium," Int. J. Numer. Methods Fluids, **59**(7), pp. 791–799.
[2] Hill, A. A., and Straughan, B., 2010, "Stability of Poiseuille Flow in a Porous Medium," *Advances in Mathematical Fluid Mechanics*, R. Rannacher and A. Sequeria, eds., Springer, Berlin, pp. 287–293.
[3] Straughan, B., and Harfash, A. J., 2013, "Instability in Poiseuille Flow in a Porous Medium With Slip Boundary Conditions," Microfluidics Nanofluidics, **15**(1), pp. 109–115.
[4] Bera, P., and Khalili, A., 2006, "Influence of Prandtl Number on Stability of Mixed Convective Flow in a Vertical Channel Filled With a Porous Medium," Phys. Fluids, **18**(12), p. 124103.
[5] Chandrasekhar, S., 1961, *Hydrodynamic and Hydromagnetic Stability*, Clarendon Press, Oxford, UK.
[6] Alchaar, S., Vasseur, P., and Bilgen, E., 1995, "Effect of a Magnetic Field on the Onset of Convection in a Porous Medium," Heat Mass Transfer, **30**(4), pp. 259–267.
[7] Bhadauria, B. S., 2008, "Combined Effect of Temperature Modulation and Magnetic Field on the Onset of Convection in an Electrically Conducting-Fluid-Saturated Porous Medium," ASME J. Heat Transfer, **130**(5), p. 052601.
[8] Bhatta, D., Muddamallappa, M. S., and Riahi, D. N., 2010, "On Perturbation and Marginal Stability Analysis of Magnetoconvection in Active Mushy Layer," Transp. Porous Media, **82**(2), pp. 385–399.
[9] Roberts, P. H., 1969, "Electrohydrodynamic Convection," Q. J. Mech. Appl. Math., **22**(2), pp. 211–220.
[10] Takashima, M., and Aldridge, K. D., 1976, "The Stability of a Horizontal Layer of Dielectric Fluid Under the Simultaneous Action of a Vertical DC Electric Field and a Vertical Temperature Gradient," Q. J. Mech. Appl. Math., **29**(1), pp. 71–87.
[11] Char, M. I., and Chiang, K. T., 1994, "Boundary Effects on the Bénard–Marangoni Instability Under an Electric Field," Appl. Sci. Res., **52**(4), pp. 331–354.
[12] Shivakumara, I. S., Nagashree, M. S., and Hemalatha, K., 2007, "Electroconvective Instability in a Heat Generating Dielectric Fluid Layer," Int. Commun. Heat Mass Transfer, **34**(9–10), pp. 1041–1047.
[13] Yabe, A., Mori, Y., and Hijikata, K., 1996, "Active Heat Transfer Enhancement by Utilizing Electric Fields," Annu. Rev. Heat Transfer, **7**, pp. 193–244.
[14] Lai, F. C., and Lai, K. W., 2002, "EHD-Enhanced Drying With Wire Electrode," Drying Tech., **20**(7), pp. 1393–1405.
[15] Moreno, R. Z., Bonet, E. J., and Trevisan, O. V., 1996, "Electric Alternating Current Effects on Flow of Oil and Water in Porous Media," K. Vafai and P. N. Shivakumar, eds., Proceedings of the International Conference on Porous Media and Their Applications in Science, Engineering and Industry, pp. 147–172.
[16] Rudraiah, N., and Gayathri, M. S., 2009, "Effect of Thermal Modulation on the Onset of Electrothermoconvection in a Dielectric Fluid Saturated Porous Medium," ASME J. Heat Transfer, **131**(10), p. 101009.
[17] Shivakumara, I. S., Rudraiah, N., Lee, J., and Hemalatha, K., 2011, "The Onset of Darcy–Brinkman Electroconvection in a Dielectric Fluid Saturated Porous Layer," Transp. Porous Media, **90**(2), pp. 509–528.
[18] Landau, L. D., and Lifshitz, E. M., 1960, *Electrodynamics of Continuous Media*, Pergamon Press, New York.
[19] Takashima, M., and Hamabata, H., 1984, "The Stability of Natural Convection in a Vertical Layer of Dielectric Fluid in the Presence of a Horizontal AC Electric Field," J. Phys. Soc. Jpn., **53**(5), pp. 1728–1736.
[20] Korpela, S. A., Gozum, D., and Baxi, C. B., 1973, "On the Stability of the Conduction Regime of Natural Convection in a Vertical Slot," Int. J. Heat Mass Transfer, **16**(9), pp. 1683–1690.
[21] Bergholz, R. F., 1978, "Instability of Steady Natural Convection in a Vertical Fluid Layer," J. Fluid Mech., **84**(4), pp. 743–768.
[22] Nield, D. A., Junqueira, S. L. M., and Lage, J. L., 1996, "Forced Convection in a Fluid Saturated Porous Medium Channel With Isothermal or Isoflux Boundaries," Proceedings of the 1st International Conference on Porous Media and Their Applications in Science, Engineering and Industry, Kona, HI, pp. 51–70.
[23] Givler, R. C., and Altobelli, S. A., 1994, "Determination of the Effective Viscosity for the Brinkman–Forchheimer Flow Model," J. Fluid Mech., **258**, pp. 355–361.